Photocatalytic Reactor Employing Titanium Dioxide: From a Theoretical Model to Realistic Experimental Results

Roberto L. Romero,* Orlando M. Alfano, and Alberto E. Cassano

Instituto de Desarrollo Tecnológico para la Industria Química (INTEC), Universidad Nacional del Litoral and CONICET, Güemes 3450, S3000GLN Santa Fe. Argentina

The performance of a reacting system for degradation of trichloroethylene (TCE) in a pilot-size annular photocatalytic reactor having a tubular lamp located at its centerline was studied. The reactor operation was carried out with commercial catalytic particles of titanium dioxide (Aldrich) in a water suspension. The description of the reactor performance was made by employing a kinetic model developed in a laboratory reactor of different size and configuration, irradiated with similar lamps of lower output power. The annular reactor was operated in the continuous mode but inside the loop of a recirculation system.The performance of the annular reactor was modeled by assuming three different behaviors: (i) a well-stirred tank reactor, (ii) a pseudo-steady-state laminar flow reactor in a batch recycle, and (iii) a transient-state laminar flow reactor in a recycle. Case iii produced the best representation of the experimental data. Along with the experimental validation of the developed theoretical models, three practical features were unveiled that had to be taken into account in any subsequent design: (a) an important change in the pH, from 6.5 to 3.5, along the reaction time; (b) a significant titanium dioxide deposition on the reactor walls; and (c) an appreciable catalyst agglomeration produced by the recirculation system and magnified by the change in pH. Only after the first 120 min of reaction time, the reactor conditions became almost stabilized; thus, the observed transformations had to be incorporated into the modeling.

I. Introduction

Catalytic reactions produced by irradiated particles of titanium dioxide, leading to the decomposition of a wide range of organic compounds, is a well-known phenomenon and has been the subject of a very long list of research work from the chemistry viewpoint.[1−3] In most of the cases, applications were made to pollutant abatement. A dissimilar occurrence can be noticed concerning quantitative studies aimed at developing useful tools for photocatalytic reactor design. Even more scarce are those contributions that attempt to report methods based on the fundamental principles of chemical reaction engineering and radiation transport theory, avoiding the use of empirical or semiempirical approximations.[4]

Employing artificial light in a continuous flow reactor, the annular geometry is perhaps the most simple and, at the same time, efficient reacting system. An exception may be a reactor with a similar geometry employing baffles located at the reaction space outer wall, to produce turbulence and improve mixing in the radial direction. A few studies have been made concerning the annular geometry, both theoretical and experimental. Sgalari et al.[5] solved the radiant field in an annular, heterogeneous photocatalytic reactor using the discrete ordinate method[6] and compared the numerical results with those obtained by application of the Monte Carlo technique. The effect produced by the radiant energy absorbed by the photocatalyst was also studied by Salaices et al.[7] using phenol as a model compound and, at the same time, proposing an experimental method to evaluate the photon absorption rate and the extinction coefficient by a titanium dioxide in the suspension. Salaices et al.[8] used the same reactor to report a particle agglomeration phenomenon that affected the extinction coefficient previously measured. A different approach was employed by Pareek et al.[9,10] to study the kinetics of the photocatalytic degradation of spent Bayer liquor in a pilot-scale, annular, bubble column reactor. They described the obtained results by employing computational fluid dynamics (CFD) methods to simulate the reactor performance. Jeon et al.[11] published an experimental study of the photocatalytic degradation of TCE by employing Degussa P 25 titanium dioxide in an internal circulating slurry bubble column reactor, reporting the effects of changes in initial TCE concentration, the flow rate of the circulating suspension, and the gas velocity in the reactor performance. In addition, the photocatalytic degradation of herbicides was studied both theoretically and experimentally by Toepfer et al.[12] and by Li Puma and Brucato.[13] These authors simplified the governing equations (fluid dynamics and radiation field) to provide a simpler method for designing photocatalytic reactors. The fountain photocatalytic reactor[14] is another configuration building on the conventional slurry reactor design that combines minimal mass-transfer limitations and no reactor wall deposits, with a very large illumination surface area per unit catalyst suspension volume. More recently, Qazaq et al.[15] utilized a bubble column reactor to investigate the photoremediation of a municipal solid waste muddy, brownish leachate.

In all of these studies knowledge of the radiant field, i.e., the specific radiant intensity at each point of the reaction space and for all possible directions of irradiation [$I_\lambda(\underline{x},\underline{\Omega})$] (a six-variable property) is essential because the photon absorption rate by the catalyst is the responsible phenomenon for initiating the degradation reaction. In fact, the reaction rate of the primary or initiation step to produce the charge separation into electrons and vacancies can be described by the product of the local volumetric rate of photon absorption [LVRPA, $e^a_\lambda(\underline{x})$], a strong function of position that is directly related to the specific intensity, and a primary quantum yield (Φ^{init}) for charge separation and transport to the catalyst surface. Under conditions of chemically and mechanically stable catalytic particles, and when all the involved reactants and products do not absorb radiation in the employed radiation wavelength range, the value

* To whom correspondence should be addressed. E-mail: tatin@santafe-conicet.gov.ar. Fax: +54 342 4511087.

10.1021/ie900354y CCC: $40.75
Published on Web 10/23/2009

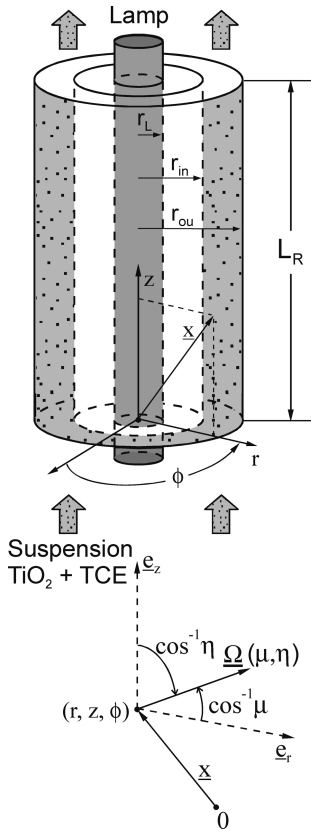

Figure 1. Reactor geometry and coordinate system corresponding to the reaction apace (adapted from Romero et al.[16]).

of $e^{a}_{\lambda}(\underline{x})$ is independent of the reaction extent. Consequently, it can be safely assumed that, a priori, it is only a function of the employed catalyst and independent of any other property of the reaction and/or reactor under analysis. In a previous work[16] the radiation field in this reactor−catalyst system employing Aldrich titanium dioxide was modeled and validated with experimental data. These results were the first evidence that the mechanical stability of the catalyst is not immediately obtained and that the characteristics of the reactor walls were almost stable only after an initial period of catalyst sticking on the reactor surfaces. It is interesting to note that in the majority of previous reports, no considerations were made concerning these effects. This is even more surprising since, more often than not, Degussa P 25 titanium dioxide catalyst was used and adhesion on reactor walls by this catalyst is even more significant.[17]

This work proposes a more realistic representation of the reactor performance. The model of the reactor to produce the photocatalytic decomposition of TCE in aqueous solution was successively modified to account for two practically observed phenomena: (i) the catalyst deposition on the reactor walls and (ii) the change in the optical properties of the catalyst as a consequence of changes in the particle sizes, resulting from two causes: (ii-a) the change in pH during the reaction and (ii-b) the agglomeration produced by the fluid recirculation in the recycle from the tank to the reactor. The employed kinetics was the one previously obtained by Brandi et al.[18] in a very different reactor configuration.

II. Experiments

II.1. Reactor Setup and Operating Conditions. The reactor was a 0.70 m long annular space, surrounding a 1.50 m tubular lamp (Philips TL 80W/09) with superficial emission (Figure 1). The reactor walls were made of borosilicate glass, which filtered any radiation wavelength below 285 nm. It was surrounded by a second annular space for ensuring constant temperature inside the reactor (20 °C) by a high flow rate circulating distilled water in a closed circuit (Figure 2). The flow reactor that was part of a recirculation, batch system complemented with a large-volume, well-stirred tank and a high flow rate centrifugal pump (QVF) was operated in laminar flow. The pump outlet stream was divided between the reactor and a second recirculation loop to improve mixing in the tank and good catalyst homogeneous distribution that translated to the whole system. A low flow rate oxygen feed was continuously added to the tank to make sure that oxygen concentration was always above the stoichiometric demand. Verification was made that the precautions taken to avoid TCE stripping were efficiently accomplished. All the connecting tubes were made of glass. The tank and all the connecting lines were covered with black adhesive tape to avoid that laboratory light altered the operating conditions. An opaque, black, cylindrical shell of threadlike fabric masked the cylindrical lamp the entire required time to achieve steady-state operation in temperature, flow rate, and lamp operation, etc., in the whole system (approximately 1 h). The zero reaction time was counted from the time that the mask was removed. The tubular lamp had a superficial emission within the wavelength range of 310−455 nm. In this way the operating domain for the reactor was between 310 and 385 nm because above this wavelength absorption by titanium dioxide is absent.

A suspension of Aldrich (Catalog No. 23,2033; Lot No. 10908 DZ; CAS No. [1317-70-0]) titanium dioxide (99% Anatase; surface area $\cong$ 9.6 m^2 g^{-1}) in concentrations always less than or equal to 1×10^{-3} g mL^{-1} circulated through the reactor annular space. As compared with Degussa P 25, for example, we are aware that Aldrich catalyst is not the best choice concerning degradation yields; however, to be consistent with our previous work,[16,18−20] we decided to use the same catalyst batch. Considering the objectives of this work (photocatalytic reactor modeling), it was understood that this selection was not a critical restraint. It has already been shown[18,19] that TCE does not absorb radiation above 285 nm. In this suspension, concentrations of TCE (Carlo Erba, RSE, 99.9%) below 70 mg L^{-1} were always employed. The concentration of TCE was measured in the tank (corresponding to the value $C^{ou}_{TCE,Tk}$) employing gas chromatography (Hewlett-Packard Model 5890 series II) with flame ionization detectors and a 60 cm long Porapak Q-S column. More details on the equipment can be found in Table 1.

To have a precise quantification of the reactor wall deposition and, at the same time, to keep a continuous monitoring of the optical properties of the suspension that is recirculating, measurements of the radiation fluxes coming out of the reactor external wall were made. These measurements were performed with a radiometer (IL 1700 from International Light) and a sensor (SED005 from the same manufacturer). The sensor included a filter with a peak at 350 nm (WBS320). It was placed at the point of measurement, employing an optical fiber made of quartz (FFO2500 from International Light). The fiber was placed at the external side of the tubular system and perpendicular to the radiation source. It could be placed in seven reproducible axial positions and six reproducible angular positions. It provided almost point measurements of the outgoing radiant flux in terms of current intensities, which can be transformed into radiation fluxes for the whole wavelength range of radiation according to the procedure described in details by Brandi et al.[21,22] Spectrophotometric extintance measurements in the range from 275 to 405 nm were made with a double-

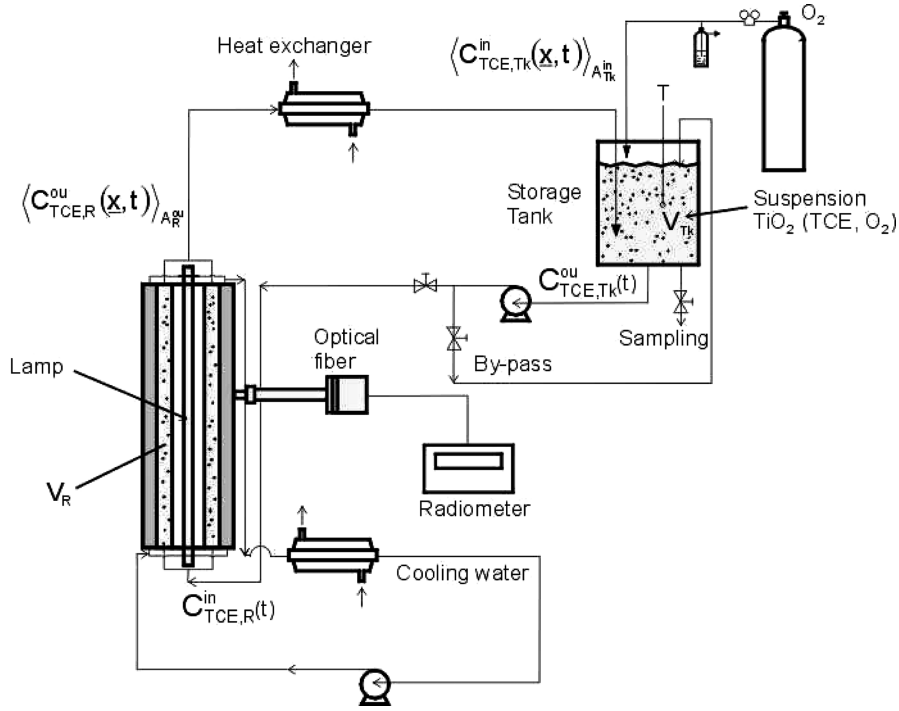

Figure 2. Experimental setup.

Table 1. Description of the Reacting System

system	detail	parameter	value
annular reactor	borosilicate glass walls	r_{in}	3 cm
		r_{ou}	4 cm
		L_R	70 cm
external annulus	borosilicate glass walls	r_{in}	4.25 cm
		r_{ou}	4.95 cm
batch recycle	total volume	$V_T = V_R + V_{Tk}$	12500 mL
	flow rate	Q	9960 mL min^{-1}
tubular lamp	nominal power	P_N	80 W
Philips TL/09	nominal arc length	L_N	150 cm
emission: superficial and diffuse	lamp radius	r_L	1.9 cm
	actual useful length	L_L	70 cm
	actual useful power	P_L	37.34 W
wavelength emission		310−445 nm	
useful emission range	considering lamp and catalyst	310−385 nm	
photochemical power	considering total lamp emission	5.9×10^{-3} einstein s^{-1}	

beam Cary 17D UV−visible spectrophotometer, using two cells having a 2 mm optical path.

II.2. Experimental Procedure. Some changes had to be made with respect to previous work due to the size of this equipment.[18,19] A 1076 mg L^{-1} saturated solution of TCE[23] was prepared from a small volume of TCE added to 1000 mL of pure water (18 MΩ). After vigorous stirring it was left for 12 h at 20 °C in a cryothermostatic bath (LAUDA K2R).

An experimental run started by filling the tank with pure water (a total volume of tank plus reactor equal to 12500 mL), which was then saturated with a stream of pure oxygen during 30 min at 20 °C. The lamp was turned on; it took an additional equal time to reach steady-state operation. With the fiber optics located at the middle axial position of the reactor length, it was possible to measure a point value of the outgoing radiation flux from the reactor and verify the stable operation of the lamp and the starting value of the radiation field with clean reactor walls. Afterward, the required amount of aqueous suspension of TiO_2, previously sonicated for 1 h was added. The suspension was circulated for at least 15 min, a time that was sufficient to register, with the optical fiber measurements, the effect in the increasing transmittance produced by the catalyst agglomeration.[16] Afterward, the lamp was covered with the opaque, black, cylindrical shell of threadlike fabric. Then, the bubbling with O_2 was stopped, and the system was maintained under overpressure of oxygen to guarantee the renewal of the oxygen consumed by the photochemical reaction. The required exact amount of TCE was added to the system, which remained under recirculation in the dark for not more than 30 min to permit adsorption of TCE, by titanium dioxide. TCE concentrations were measured in several samples at 10 min intervals, until the measurement gave a constant value (the sample volume was always 10 cm^3). The black cylindrical shell was retired, and this was registered as the reaction time equal to zero. During all the time occurring from the moment in which the titanium dioxide was added, measurements with the fiber optics and samples taken from the tank were used to measure the extinctance of the suspension (absorption plus scattering effects). The lamp operation was controlled with a V-A-W meter.

Once the photocatalytic run was finished (approximately 5 h of reaction), the total system was gently washed by employing pure water. This procedure permitted the elimination of all the catalytic suspension, keeping the reactor walls always wetted. With this programmed method it was intended to keep the reactor wall deposition unaltered. The wash progressed up to the point where the readings in the radiometer as well as the extinctance measurements of the outgoing water were constant. This operation took about 1 h. At this moment, it was possible to make a separate measurement of the loss of transmission produced by the reactor walls deposition, separately from the effect produced by the catalyst agglomeration. Measurements were made moving the optical fiber axial and angular manner.[16] The angular values showed differences always smaller than 5% and were averaged at its axial position, allowing a one-dimensional functional representation of the nonuniform axial profile along the reactor length.

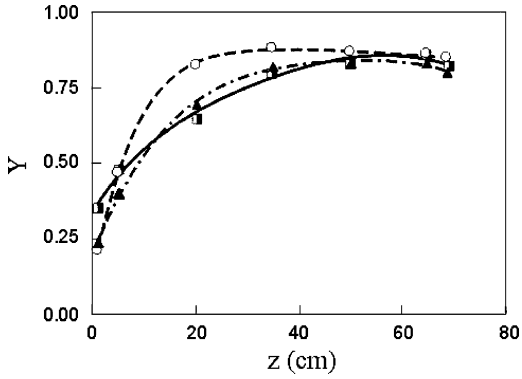

Figure 3. Longitudinal profiles describing the reactor wall deposition: $C_{m,cat.} = 0.25 \times 10^{-3}$ g mL^{-1} and $C^0_{TCE} = 65.08$ mg L^{-1}, experimental data (◨) and interpolation line (−); $C_{m,cat.} = 0.50 \times 10^{-3}$ g mL^{-1} and $C^0_{TCE} = 65.08$ mg L^{-1}, experimental data (○) and interpolation line (--); $C_{m,cat.} = 1.0 \times 10^{-3}$ g mL^{-1} and $C^0_{TCE} = 68.43$ mg L^{-1}, experimental data (▲) and interpolation line (- • -).

III. Reactor Wall Deposition

The attachment by titanium dioxide to the walls produced an extra and thin layer of catalyst on the reactor walls. Consequently, due to the high radiation absorption by titania, a given absorbance can be assigned to it that will affect the radiant field of the whole system. The radiometer measurements described before permitted one to obtain an axial profile of the loss of transmittance produced by the wall deposition. Due to the very small vision angle of the optical fiber (23° is the average reception angle for the wavelength range of 310−410 nm, reported by Brandi[24]) it is possible to assume that these measurements represented true axial, local values of the radiant fluxes arriving at the external wall of the annular reaction space. Consequently it could also be assumed that the rays coming out in this direction perpendicular to the radiation source are the ones that also correspond to the radiation rays that are entering the reactor inner wall in a direction practically normal to it. If we accept the hypothesis that the deposition is the same in both inner walls of the annular space, then the same radiation absorption (loss of transmission) would be developed in both surfaces. Thus, from measurements of the clean reactor walls and the ones having the stuck titanium dioxide, it will be possible to obtain a longitudinal profile of the real transmittance resulting from the catalytic deposition on the surfaces. Figure 3 shows the results obtained for the axial profiles corresponding to the actual transmittance resulting from the observed deposit in experiments conducted at three different TiO_2 concentrations. The transmittance values are kept almost constant at 80% with the exception of the inlet section of the reactor (up to almost the middle height position) that shows a more significant deposition, probably due to the effects produced by the flow distributor to the suspension impinging at the wall close to this section. This effect, somehow diminished, was observed at the reactor outlet. As compared with the magnitude of the reaction occurring in the slurry, the eventual wall catalytic reaction produced by the phenomenon was neglected.

IV. Optical Properties Variations

The existence of agglomeration in the catalytic particles has been reported before.[8,16,18] This circumstance produces an important change in the catalyst optical properties. These changes were attributed to two causes: (a) stirring and recirculation and (b) variations in pH. In principle, agitation and recirculation have been shown to produce an increase in the

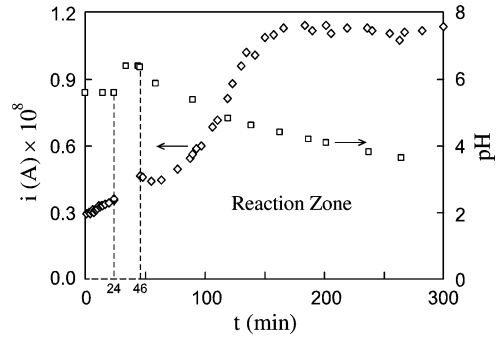

Figure 4. pH variations (□) and radiometer readings of measurements made with the fiber optics in terms of current intensities (◊). Measurements were made at the reactor middle height position and at a constant angular position. $C_{m,cat.} = 0.50 \times 10^{-3}$ g mL^{-1}; $C^0_{TCE} = 35.75$ mg L^{-1}.

transmittance of the suspension that is proportional to the time evolution of the system. This phenomenon was reported by Romero et al.[16] in the absence of chemical reaction. On the other hand, the reaction mixture changes from pH 6.5 at the beginning of the reaction to a final value of approximately pH 3.5, corresponding to the reached conversion after 4 or 5 h of reaction time (see data in Figure 4). This effect produces a nonlinear change in the transmittance of the suspension.[18] In Brandi et al.'s work,[18] changes in transmittance were translated directly into the extinctance of the suspension, considering that the main effect was produced by modifications in scattering resulting from the increasing size of the particles. Work reported latter by Satuf et al.[25] have shown that all optical properties are utterly different from pH 6.5 to pH 2.5. In our case, the specific extinctance (β^*_λ) was measured in the suspension (from samples in the tank) with a spectrophotometer and the changes in the specific absorption coefficient were obtained by an optimization procedure as described in what follows.

As mentioned before, during the experimental work, changes in the radiant field (more specifically, transmissions) were continuously monitored with fiber optics located at the middle height position of the external reactor wall. Figure 4 shows the temporal variations during a typical run. The data were expressed directly in current intensities to avoid, at this point, unnecessary transformations. The reasons for this direct approach are the following: According to Brandi et al.[22] one could transform the radiometer readings in current intensities into the desired radiative fluxes employing the following information and steps: (i) the absolute sensitivity of the instrument at a specified wavelength (given by the sensor manufacturer's specifications); (ii) the sensor sensitivity relative spectral wavelength distribution (given by the sensor manufacturer's specifications); (iii) the value of the relative spectral distribution of the arriving polychromatic flux at the surface of the detector. The first two steps do not present major difficulties. The third one has the following drawbacks: (1) In the first place, to have an accurate representation of the wavelength distribution of the arriving energy, it is necessary to resort to a hypothesis concerning the wavelength distribution of the lamp output. This implies the acceptance of the existence of no deviations from the technical information provided by the lamps' manufacturer. (2) The transmittance of both reactor wall experiments changes with time as it is described in the following sections. (3) Between both walls, there is a titanium dioxide suspension that absorbs and scatters radiation, varying the wavelength distribution of the lamp output. To avoid these uncertainties, to estimate the different physical effects measured with the radiometer, the direct use of current intensities does not introduce any distortion

in the results. The use of them in the different parameter estimations permits the correct interpretation of the experimental data without distortion or difficulties.

At the beginning, with the system irradiated and the TiO_2 suspension exclusively flowing, Figure 4 shows a linear variation of the transmitted radiation during 24 min. This behavior is similar to the one observed by Romero et al.[16] without chemical reaction. This is the effect produced by agitation and recirculation. Afterward, there is a dark region (between 24 and 46 min), corresponding to the addition of TCE in the absence of radiation (recall and compare with the previous description of the initiation of an experimental run). Finally, when the reaction begins at time equal to 46 min, a nonlinear variation in the results of these measurements can be observed. This is a combined effect of mechanical stirring and change in the solution pH.[18] As shown in Figure 4, changes in pH along the reaction evolution are significant and this effect cannot be ignored.

Simultaneously, for each run, samples in the tank were taken with a 2-fold purpose: (a) chemical analysis and (b) spectrophotometric measurements of extinctance. The range of 275−405 nm was swept in both directions in the spectrophotometer, and the highest values at the same wavelength were taken as valid in consideration of possible settling of the larger particles. More details on these experiments can be seen in Cabrera et al.[26] and Satuf et al.[20]

From the values of β_λ^*, it is possible to think that all these changes were the result of variations in the scattering coefficient (σ_λ^*) produced by the increasing size of the scattering centers as supposed by Brandi et al.,[18] i.e., that the absorption coefficient κ_λ^* remains constant. However, when these sole values of the optical properties were used to predict theoretically the evolution of the measurements made with the optical fiber outside the reactor wall, the experimental values were not reproduced. They were systematically higher than all theoretical predictions with the previous assumption. It is then reasonable to think that also the absorption coefficient was changed and that it may have been significantly reduced.[8,25] These results can be interpreted as the consequence of an important decrease in radiation absorption by larger particles.[27]

Consequently, the corrected values employed in this work were obtained by optimization. Using the experimental data of $\beta_\lambda^*(t)$, the optimization software provides the $\kappa_\lambda^*(t)$ values which minimize the differences between the experimental measurements obtained from the optical fiber and the theoretical predictions. In this way it was possible to obtain the pair of absorption and scattering coefficients as a function of wavelength and time [$\kappa_\lambda^*(t)$ and $\sigma_\lambda^*(t)$] employed in this work. No changes in the phase function were made.[20] These aspects introduce some differences with the interpretation of the experimental results made by Brandi et al.[18]

It must be noted that both κ_λ^* and σ_λ^* are a function of the reaction time and give coherence to the experimental values measured with the fiber optics along this time. Figure 5 shows the values of $\beta_\lambda^*(t)$ and $\kappa_\lambda^*(t)$ as a function of time for a typical run. As expected, the extinction coefficient measured with the spectrophotometer shows a different trend as compared with the radiation field measured with the optical fiber (cf. with data plotted in Figure 4); however, considering the remarkably different meaning of both physical properties, the observed results are fully consistent. The absorption coefficients by the suspension measured by Satuf et al.[20] at pH 6.5 decrease to our values obtained by optimization at values around pH 3.5 at the end of the experimental run and are in accordance with a similar evolution reported in the measurements made by Satuf et al.[25] at pH 2.5.

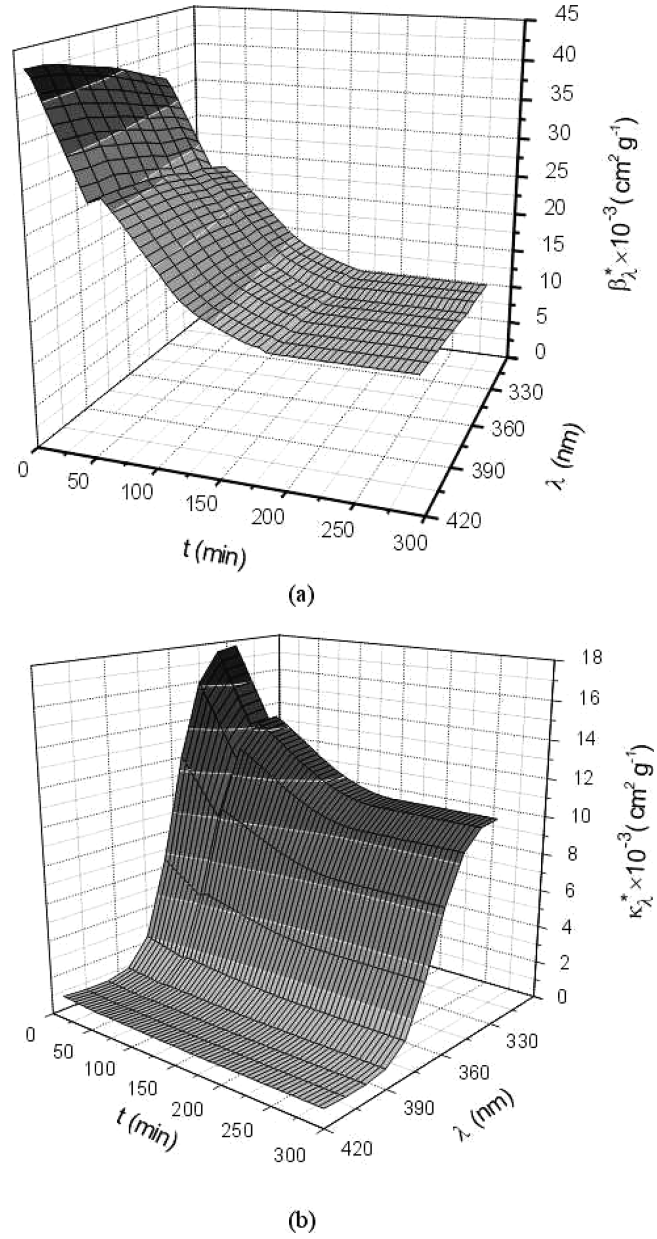

Figure 5. Agglomeration. Temporal evolution of optical parameters: $C_{m,cat.} = 0.50 \times 10^{-3}$ g mL^{-1}; $C_{TCE}^0 = 35.75$ mg L^{-1}; (a) $\beta_\lambda^*(t)$ and (b) $\kappa_\lambda^*(t)$.

V. Reactor Modeling

V.1. Theory. For the temporal variation of the TCE concentration in the system, separate mass balances were written for the tubular reactor and for the tank. The storage tank works always under perfect stirring conditions and in the transient state. The mass balance for species i (TCE) is given by

$$\varepsilon_L \frac{dC_{i,Tk}^{ou}(t)}{dt} = \frac{Q}{V_{Tk}}[\langle C_{i,Tk}^{in}(\underline{x}, t)\rangle_{A_{Tk}^{in}} - C_{i,Tk}^{ou}(t)] \quad (1)$$

$$C_{i,Tk}^{ou}(t = 0) = C_i^0 \quad (2)$$

The incoming concentration in the tank is the one issued from the tubular reactor outlet. To know this concentration, the mass

balance for the annular reactor must be written. Considering a two-dimensional, pseudohomogeneous reactor, under laminar flow and un-steady-state regime,

$$\varepsilon_L D_{i,\mathrm{mix}}\left[\frac{\partial^2 C_{i,R}(r,z,t)}{\partial r^2}+\frac{1}{r}\frac{\partial C_{i,R}(r,z,t)}{\partial r}\right]- \varepsilon_L v_z(r)\frac{\partial C_{i,R}(r,z,t)}{\partial z}+\nu_i a_V \boldsymbol{R}_{\mathrm{het}}(r,z,t)=\varepsilon_L\frac{\partial C_{i,R}(r,z,t)}{\partial t} \quad (3)$$

$$\begin{aligned} z=0 &\rightarrow C_{i,R}(r,z=0,t)=C^{\mathrm{ou}}_{i,\mathrm{Tk}}(t)\\ r=r_{\mathrm{in}} &\rightarrow \frac{\partial C_{i,R}}{\partial r}(r=r_{\mathrm{in}},z,t)=0\\ r=r_{\mathrm{ou}} &\rightarrow \frac{\partial C_{i,R}}{\partial r}(r=r_{\mathrm{ou}},z,t)=0\\ t=0 &\rightarrow C_{i,R}(r,z,t=0)=C^0_{i,R} \end{aligned} \quad (4)$$

The solution of this equation will provide the value of the average exit concentration from the reactor:

$$\langle C^{\mathrm{ou}}_{i,R}(r,z=L_R,t)\rangle_{A^{\mathrm{ou}}_R}=\frac{\int_0^{2\pi}\int_{r_{\mathrm{in},R}}^{r_{\mathrm{ou},R}} C_{i,R}(r,L_R,t)\,v_z(r)r\,\mathrm{d}r\,\mathrm{d}\theta}{\int_0^{2\pi}\int_{r_{\mathrm{in},R}}^{r_{\mathrm{ou},R}} v(r)r\,\mathrm{d}r\,\mathrm{d}\theta}= \langle C^{\mathrm{in}}_{i,\mathrm{Tk}}(\underline{x},t)\rangle_{A^{\mathrm{in}}_{\mathrm{Tk}}} \quad (5)$$

This is the most rigorous approach. To compare results, two other operation descriptions can be considered. The first is an approximation and the second a limiting case:

The first estimate, assumes that the tubular reactor operates under steady state and consequently

$$\varepsilon_L D_{i,\mathrm{mix}}\left[\frac{\partial^2 C^{\mathrm{t}}_{i,R}(r,z)}{\partial r^2}+\frac{1}{r}\frac{\partial C^{\mathrm{t}}_{i,R}(r,z)}{\partial r}\right]-\varepsilon_L v_z(r)\frac{\partial C^{\mathrm{t}}_{i,R}(r,z)}{\partial z}+ \nu_i a_V \boldsymbol{R}^{\mathrm{t}}_{\mathrm{het}}(r,z)=0 \quad (6)$$

$$z=0\rightarrow C^{\mathrm{t},0}_{i,R}(r,z=0)=C^{\mathrm{ou}}_{i,\mathrm{Tk}}(t) \quad (7)$$

where the reactor incoming reactant concentration shows a parametric dependence with respect to time, as it is represented by eq 7.

The second one assumes that the operation of the complete system is as follows: (a) there is a transient state; (b) there are well-stirred conditions; (c) $V_R << V_{\mathrm{tot.}} = V_R + V_{\mathrm{Tk}}$, where $V_{\mathrm{Tk}} = V_{\mathrm{tot.}} - V_R$; and (d) the reactor operates under almost differential conversion per pass. Under these conditions, it can be shown that[28]

$$\varepsilon_L\frac{\mathrm{d}C^{\mathrm{ou}}_{i,\mathrm{Tk}}(t)}{\mathrm{d}t}=\frac{V_R}{V_{\mathrm{tot.}}}a_V\langle\nu_i\boldsymbol{R}_{\mathrm{het}}(\underline{x},t)\rangle_{a_V V_R} \quad (8)$$

$$C^{\mathrm{ou}}_{i,\mathrm{Tk}}(t=0)=C^0_i \quad (9)$$

Under these assumptions, the result produces the limiting case of a single, well-stirred, batch system.

The employed reaction rate was taken from Brandi et al.:[18]

$$\nu_i\boldsymbol{R}_{\mathrm{het}}(\underline{x},t)a_V= -S_g(C_{\mathrm{m,cat.}})^{1/2}\alpha\left(\int_\lambda e^{\mathrm{a}}_\lambda(\underline{x},t,C_{\mathrm{m,cat.}})\,\mathrm{d}\lambda\right)^{1/2}\frac{\alpha_3 C_i(\underline{x},t)}{1+\alpha_3 C_i(\underline{x},t)} \quad (10)$$

where $\alpha = 1.94\times10^{-9}$ mol cm^{-2} g$^{1/2}$ einstein$^{-1/2}$ s$^{-1/2}$ and $\alpha_3 = 5.52\times10^6$ mL mol^{-1}. Equation 10 calls for a value of $\int_\lambda e^{\mathrm{a}}_\lambda(\underline{x},t,C_{\mathrm{m,cat.}})\,\mathrm{d}\lambda$, which implies the need to calculate $e^{\mathrm{a}}_\lambda(\underline{x},t,C_{\mathrm{m,cat.}})$. This value is obtained from the solution of the radiative-transfer equation (RTE) for each point inside the annular space and valid for monochromatic radiation (λ) and a given direction of propagation $\underline{\Omega}$. According to Romero et al.[16]

$$\underline{\nabla}\cdot[\underline{\Omega}I_\lambda(\underline{x},\underline{\Omega},t)]+\kappa_\lambda(\underline{x},t)\,I_\lambda(\underline{x},\underline{\Omega},t)+\sigma_\lambda(\underline{x},t)\,I_\lambda(\underline{x},\underline{\Omega},t)= \frac{\sigma_\lambda(\underline{x},t)}{4\pi}\int_{\Omega'=4\pi}p(\Omega'\rightarrow\Omega)\,I_\lambda(\underline{x},\underline{\Omega}',t)\,\mathrm{d}\Omega' \quad (11)$$

Equation 11 must be solved with the following boundary conditions (the most important variables and the spatial and directional coordinates are defined in Figure 1):

$$\begin{aligned} I_\lambda(r,0,\mu,\eta,t)&=I_\lambda(r,L_R,\mu,\eta,t)=0\\ I_\lambda(r_{\mathrm{ou}},z,\mu,\eta,t)&=I_{\lambda,\mathrm{Rf}}(r_{\mathrm{ou}},z,\mu,\eta,t)\\ I_\lambda(r_{\mathrm{in}},z,\mu,\eta,t)&=\mathrm{Y}_{\lambda,r_{\mathrm{in}}}I_{\lambda,\mathrm{Lp}}(r_{\mathrm{in}},z,\mu,\eta,t)+\\ &(\mathrm{Y}_{\lambda,r_{\mathrm{in}}})^2 I_{\lambda,\mathrm{bs}}(r_{\mathrm{in}},z,\mu,\eta,t)+I_{\lambda,\mathrm{Rf}}(r_{\mathrm{in}},z,\mu,\eta,t) \end{aligned} \quad (12)$$

where the following has been taken into account: (i) the lamp emission model ($I_{\lambda,\mathrm{Lp}}$), considered the presence of a three-dimensional, steady-state, superficial emission,[29] (ii) the back-scattering ($I_{\lambda,\mathrm{bs}}$) produced by the suspension at $r = r_{\mathrm{in}}$, and (iii) the reflected photons on the inner side of the internal and external reactor walls ($I_{\lambda,\mathrm{Rf}}$). It must been stressed that the emission from the lamp is the result of a theoretical model and under no circumstances an experimental actinometry has been made; this must be so because, in any realistic reactor design, the equipment to be built will not be available for these measurements. For more details, the reader is referred to the quoted reference.

With respect to the employed catalyst (TiO_2, Aldrich) the initial optical properties at the beginning of each run [the absorption coefficient (κ^*_λ), the scattering coefficient (σ^*_λ), and the phase function $p_\lambda(\Omega'\rightarrow\Omega)$] were taken from recent measurements made by Satuf et al.[20] at pH = 6.5. Afterward, when the agglomeration and the change in pH take place, the values of κ^*_λ and σ^*_λ were calculated as it was explained before. From the field of specific radiation intensities, $[I_\lambda(\underline{x},\underline{\Omega},t)]$, obtained from the solutions of eqs 11 and 12, the LVRPA was calculated as follows:

$$e^{\mathrm{a}}_\lambda(\underline{x},t)=\int_{\Omega=4\pi}I_\lambda(\underline{x},\underline{\Omega},t)\,\mathrm{d}\Omega \quad (13)$$

In addition, the polychromatic LVRPA results:

$$e^{\mathrm{a}}(\underline{x},t)=\int_\lambda e^{\mathrm{a}}_\lambda(\underline{x},t)\,\mathrm{d}\lambda \quad (14)$$

It must be noticed, as it was indicated in eq 9, that $e^{\mathrm{a}}_\lambda(\underline{x},t) = e^{\mathrm{a}}_\lambda(\underline{x},t,C_{\mathrm{m,cat.}})$ to emphasize that the LVRPA is a strong function of the catalyst properties.

V.2. Numerical Solution. Equations 1−4 represent one system of coupled differential equations that must be solved together with the integrodifferential equation that describes the radiation field in the annular space of reaction (eqs 11−14). The solution mechanism asks for the adoption of a temporal step to characterize the system. Following Wolfrum and Turchi,[30] this time can be adopted as the mean residence time (t_R). During one residence time, the inlet concentration in the tubular reactor is considered constant. It is the parametric representation given by eq 7, where the time dependence of the said parameter is set equal to t_R. Ballari et al.[27,31] have solved the system with an approach much closer to the actual transient state, using a significantly smaller characteristic time for the

changes in the tank concentration, and, consequently, the inlet concentration in the annular reactor changes in an almost continuous fashion. Depending upon the reaction rate and the conversion per pass, both approaches may be very similar. However, with the existence of the numerical discretization procedure employed in the solution of both systems of differential equations, rigorously speaking, the outcome cannot be considered equal to a true transient state. The following steps were followed.

(1) The initial concentration of TCE (after the adsorption equilibrium has been reached) is used as the initial condition for the tank: $C_{i,\mathrm{Tk}}^{\mathrm{ou}}(t=0) = C_i^0$.

(2) The same value is the initial condition for the annular reactor: $C_{i,\mathrm{R}}(r,z,t{=}0) = C_{i,\mathrm{R}}^0$. Using a finite difference technique the concentration field in the annular reactor in the transient state is solved during the time t_{R} considering that, during this time, $C_{i,\mathrm{Tk}}^{\mathrm{ou}}$ remains constant. This allows calculation of the concentration profile at the annular reactor outlet. With this value, the cup-averaged outlet concentration $\langle C_{i,\mathrm{R}}^{\mathrm{ou}}(\underline{x},t)\rangle_{A_{\mathrm{R}}^{\mathrm{ou}}}$ is calculated, which is equal to the inlet concentration in the tank $\langle C_{i,\mathrm{Tk}}^{\mathrm{in}}(\underline{x},t)\rangle_{A_{\mathrm{Tk}}^{\mathrm{in}}}$ after t_{R}.

(3) Employing a second-order Runge−Kutta algorithm, eqs 1 and 2 are solved. This procedure, renders the new output concentration from the tank after t_{R} equal to $C_{i,\mathrm{Tk}}^{\mathrm{ou}} \neq C_i^0$.

(4) Steps 2 and 3 are repeated as many times as required to reach the total reaction time of each run.

With respect to the choice of the characteristic time interval for the transient-state solution, it must be stressed once more that, in actual terms, the whole system is operating in a permanent intrinsic transient state. The solution adopted here seems to be a logical approximation to obtain the output concentration of the annular reactor. In this particular system, variations made with smaller time intervals did not introduce significant changes in the storage tank outlet concentration. For temporal intervals greater than $\tau \cong 9$ the solution of the system becomes highly unstable.

Computation of the reaction rate (eq 10) needs the result of eq 14. This demands the value of the radiation field in the annular region, which is spatially two-dimensional (r, z) and angularly two-directional (μ, η) (recall eqs 11 and 12) and also a function of time because κ_λ^* and σ_λ^* are time-dependent. Moreover, the solution is obtained for each pseudo-monochromatic wavelength interval $\Delta\lambda$. To get the solution, the discrete ordinate method (DOM) is employed.[6] The integrodifferential equation (eq 11) is transformed into a set of algebraic equations that are solved starting from the boundary conditions (eq 12) and following the sense of radiation propagation. To apply the DOM at each reaction time (recall once more that κ_λ^* and σ_λ^* are both a function of t), three discretizations are needed: (i) for the spatial variables r and z (angular symmetry has been assumed), (ii) for the directional spherical variables $\Omega = \Omega(\mu,\eta)$, and (iii) the spectral variable in the range of useful wavelengths. The detailed procedures have been described in Romero et al.[16,32]

The solution of the system corresponding to the annular reactor under steady-state conditions implies a numerical representation in terms of a Crank−Nicholson approach together with the solution of a system of algebraic equations employing the Thomas algorithm. Since the reaction rate does not have a linear dependence with the concentration, it is necessary to iterate in the concentration field until convergence within a prescribed error is obtained.

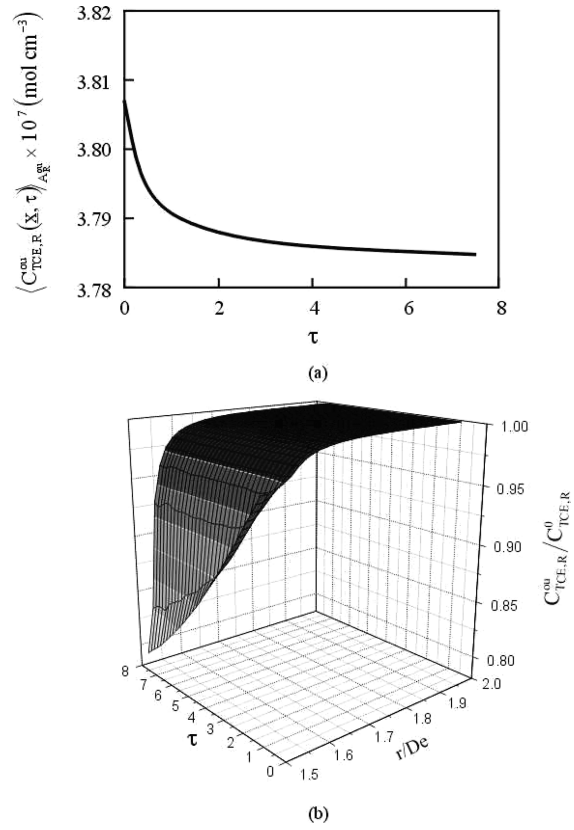

Figure 6. (a) Temporal evolution of the annular reactor outlet concentration $[\langle C_{\mathrm{TCE,R}}^{\mathrm{ou}}(\underline{x},\tau)\rangle_{A_{\mathrm{R}}^{\mathrm{ou}}}]$ considering operation of the annular reactor under constant inlet concentration. (b) Dimensionless, temporal variation of the radial profiles of TCE $C_{\mathrm{TCE,R}}^{\mathrm{ou}}(\underline{x},\tau)/C_{\mathrm{TCE,R}}^{\mathrm{ou}}$.

VI. Results

VI.1. Laminar Reactor Behavior. The employed pseudo-transient-state solution for solving the entire system, as stated before, implies that, during one residence time in the tubular reactor, the feed concentration remains constant. It seems appropriate to analyze first the transient behavior of the laminar flow reactor under the assumption that it works alone, receiving a constant concentration feed. The results of this simulation are shown in Figure 6a,b. The first shows the temporal variation of $\langle C_{\mathrm{TCE,R}}^{\mathrm{ou}}(\underline{x},t)\rangle_{A_{\mathrm{R}}^{\mathrm{ou}}}$ when the reactor is fed with an inlet concentration of TCE ($C_{\mathrm{TCE,R}}^0$) = 50 mg L^{-1} employing a catalytic suspension of 0.50×10^{-3} g mL^{-1}. There is a steep gradient in the first part of the reactor length; in the second part, the variation decreases more slowly, until the point where the steady-state concentration has been reached. The required time is approximately equal to 7.5 t_{R}. When the complete system assumes that the reactor operates at steady state, the mathematical solution should employ this time scale. As indicated before, values larger than t_{R} produce significant changes in the final value of the tank output concentration $C_{\mathrm{TCE,Tk}}^{\mathrm{ou}}$. This is a clear indication that the assumptions involved in eqs 6 and 7 are unacceptable. Figure 6b depicts the radial profiles of $C_{\mathrm{TCE,R}}^{\mathrm{ou}}/C_{\mathrm{TCE,R}}^0$ for different times under constant reactant feed. For this case, it can be seen that only the reactor layer closer to the inner radius of the reactor, i.e., closer to the tubular lamp, produces significant conversions of TCE, the reason being that 0.50×10^{-3} g mL^{-1} of catalyst concentration introduces a very high optical density in the reaction space. An irrelevant change in the radial profile is also observed in a thin layer close to the

outside diameter of the annulus, resulting from the very long residence time generated by the assumed laminar flow reactor operation.

VI.2. TCE Degradation. In a first approximation, the reacting system is solved assuming that the value of the LVRPA corresponds to a reactor with clean walls and no catalyst agglomeration, i.e., constant optical properties of the catalyst. For this purpose eqs 1−9 were solved in an increasing degree of complexity: (i) the perfectly mixed system (eqs 8 and 9), (ii) the tank performance, separately, on the one hand (eqs 1 and 2) and, on the other, the reactor, with the assumption that it operates under steady-state conditions (eqs 6 and 7), and, finally, (iii) the tank (eqs 1 and 2) linked with the reactor operating under a transient performance (eqs 3 and 4). In Figure 7a the results of the temporal evolution of $C^{ou}_{TCE,Tk}(t)$ can be observed for a typical run and for the three proposed models. The values of approximations i and ii do not show too many differences, as it has been already reported by Satuf et al.[33] Model iii shows significant variations from the other two, resulting from the more realistic assumption of the transient behavior. Notable differences after 4−5 h of one experiment are observed. Deviations for model iii fall within the range of −11.6 to −1.8%. The absolute error average value (AEAV) is 6.9% and the root square mean error (RSME) is 2.6%. Since in this case the radiation field is calculated in excess, because only "clean and initial" values of the optical properties have been used, it seems logical that all the experimental values fall above all predictions.

Theoretical predictions were compared with all experimental data [$C^{ou}_{TCE,Tk}(t)$] employing three different catalyst loadings: $C_{m,cat.}$ = (0.25, 0.50, and 1.0) × 10^{-3} g mL^{-1} and three different initial conditions of TCE ≤ 70 mg L^{-1} (Figure 8). The results with model iii indicate deviations between −38.8 and +13.1%. AEAV = 14.9%, and RSME = 2.1%.

VI.3. Reactor Walls Deposition. The deposition produces an actual decrease of the specific available intensities because the values of the boundary conditions for eq 11 (eqs 12) are correspondly changed.

When these values are taken into account in the three models, the results for a typical run are shown in Figure 7b. A shift of the theoretical predictions toward the experimental values is observed. For model iii deviations are in the range between −7.6 and +2.1%. AEAV = 3.9%, and RSME = 1.6%. Considering all the obtained experimental data (Figure 9), the results with model iii indicate deviations between −30.3 and +25%. AEAV = 11.1%, and RSME = 1.6%.

VI.4. Variation in the Optical Properties due to Agglomeration and Change in pH. In sections VI.1, VI.2, and VI.3 all calculations were made considering that the radiation field given by eq 10 was constant, only affected, in case VI.3, at the boundary conditions. The last corrections that can be made according to the experimental observations are those due to changes in pH and agglomeration; the optical properties are altered and become a function of the reaction time, i.e., $\beta^*_\lambda(t)$, $\kappa^*_\lambda(t)$, and $\sigma^*_\lambda(t)$, where t is the reaction time. The time evolution of $\beta^*_\lambda(t)$ and $\kappa^*_\lambda(t)$ have almost opposite trends, which is a clear indication that the radiation field has been changed. These changes were incorporated in the three models, and the results for the same run as before are shown in Figure 7c. The experimental results show a much better agreement; deviations fall within the interval −6.2 to +3.7%, with an AEAV value of 3.3% and a RSME value of 1.3%. Considering all of the experimental runs (Figure 10), the results according to model iii are as follows: (1) deviations between −17.8 and +34%, (2) the AEAV value is 8.5%, and (3) the RSME value is 1.26%.

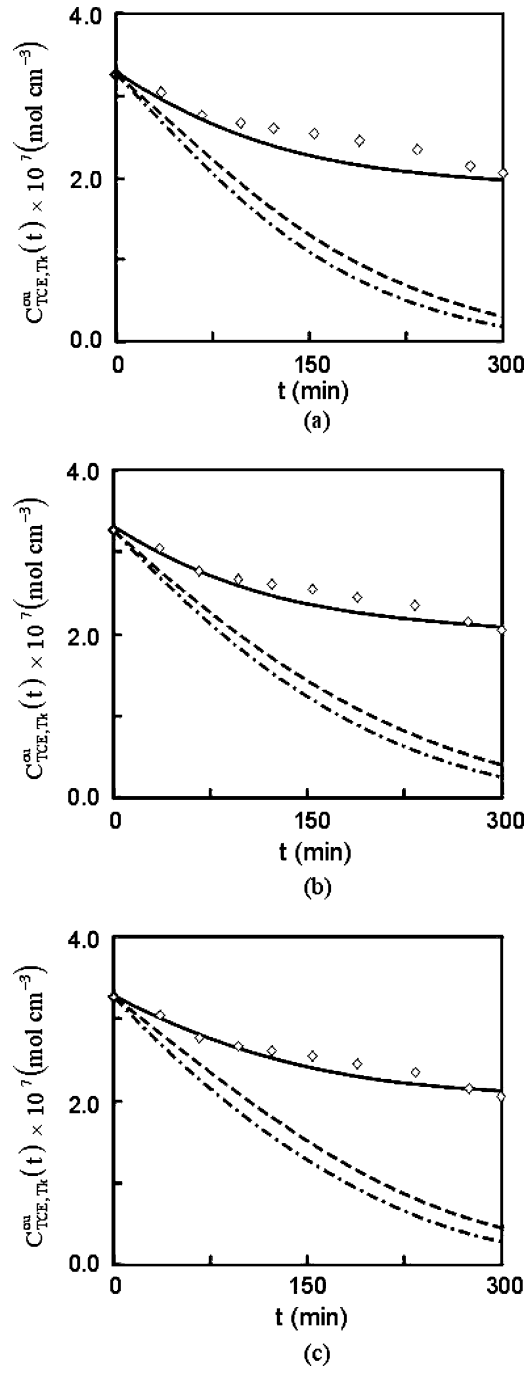

Figure 7. Temporal evolution of $C^{ou}_{TCE,Tk}(t)$. Typical results considering the following: (a) neither deposition nor agglomeration; (b) deposition and no catalyst agglomeration; (c) deposition and catalyst agglomeration: model i, − · −; model ii, --; model iii, −. Experimental data: (◇). $C_{m,cat.}$ = 0.25 g/L; C^0_{TCE} = 42.8 mg L^{-1}.

The reactor performance has been predicted reasonably well when model iii is applied. When these results are finally analyzed, it cannot be avoided to refer to the origin of the employed kinetic model (Brandi et al.[18]). In that work, the obtained kinetic parameters were calculated using a different interpretation of the agglomeration problem. Furthermore, a two-dimensions in space−two-dimensions in direction reactor model (as the one employed by Brandi et al.[18]) is not the very best configuration for obtaining kinetic parameters. Simple reactors are preferred.

The proposal of the fountain head reactor made by Li Puma and Yue[14] that has, at the same time, the possibility of being operated as an excellent solar reactor offers a solution to the

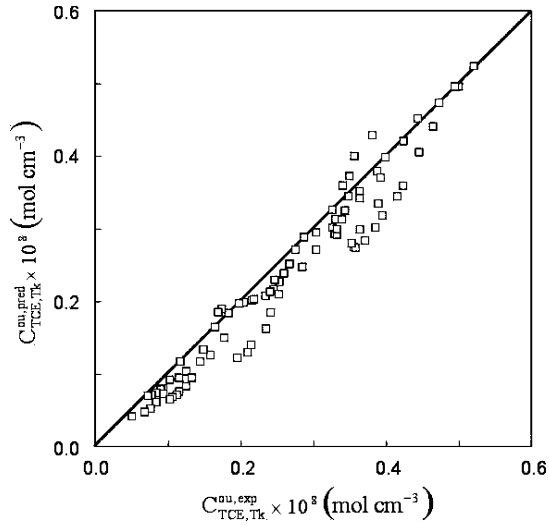

Figure 8. Results considering a reactor with clean walls and no catalyst agglomeration with model iii and all runs. Predicted values $C^{ou,pred}_{TCE,Tk}(t)$ versus experimental values $C^{ou,exp}_{TCE,Tk}(t)$. Experimental data (□): $C_{m,cat.} = 1.0$ g/L, $C^0_{TCE} = 52.32$ mg L^{-1}; $C_{m,cat.} = 0.50$ g/L, $C^0_{TCE} = 35.75$ mg L^{-1}; $C_{m,cat.} = 0.50$ g/L, $C^0_{TCE} = 65.08$ mg L^{-1}; $C_{m,cat.} = 1.0$ g/L, $C^0_{TCE} = 24.02$ mg L^{-1}; $C_{m,cat.} = 0.25$ g/L, $C^0_{TCE} = 42.8$ mg L^{-1}; $C_{m,cat.} = 0.50$ g/L, $C^0_{TCE} = 15.46$ mg L^{-1}; $C_{m,cat.} = 0.25$ g/L, $C^0_{TC} = 65.08$ mg L^{-1}; $C_{m,cat.} = 1.0$ g/L, $C^0_{TCE} = 68.43$ mg L^{-1}; $C_{m,cat.} = 0.25$ g/L, $C^0_{TCE} = 21.7$ mg L^{-1}.

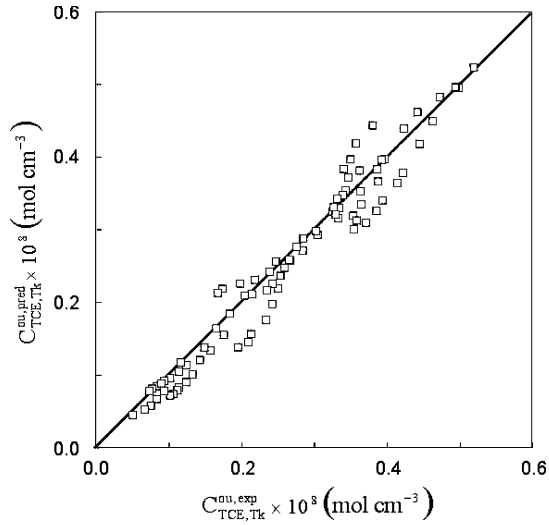

Figure 9. Results considering deposition and no catalyst agglomeration with model iii and all runs. Predicted values $C^{ou,pred}_{TCE,Tk}(t)$ versus experimental values $C^{ou,exp}_{TCE,Tk}(t)$. Experimental data (□): $C_{m,cat.} = 1.0$ g/L, $C^0_{TCE} = 52.32$ mg L^{-1}; $C_{m,cat.} = 0.50$ g/L, $C^0_{TCE} = 35.75$ mg L^{-1}; $C_{m,cat.} = 0.50$ g/L, $C^0_{TCE} = 65.08$ mg L^{-1}; $C_{m,cat.} = 1.0$ g/L, $C^0_{TCE} = 24.02$ mg L^{-1}; $C_{m,cat.} = 0.25$ g/L, $C^0_{TCE} = 42.8$ mg L^{-1}; $C_{m,cat.} = 0.50$ g/L, $C^0_{TCE} = 15.46$ mg L^{-1}; $C_{m,cat.} = 0.25$ g/L, $C^0_{TCE} = 65.08$ mg L^{-1}; $C_{m,cat.} = 1.0$ g/L, $C^0_{TCE} = 68.43$ mg L^{-1}; $C_{m,cat.} = 0.25$ g/L, $C^0_{TCE} = 21.7$ mg L^{-1}.

catalyst deposition effect; however, agglomeration produced in the solid particles during the reactor operation remains as an unsolved problem that cannot be ignored for the slurry operation.

VII. Conclusions

(1) The obtained results have confirmed previous studies[16] that have shown that realistic reactors, employing titanium dioxide during a reasonably long reaction time, have a performance that is very different than the one predicted by purely theoretical calculations.

(2) A reaction−reactor model has been used with reasonable success in the interpretation of realistic experimental data for

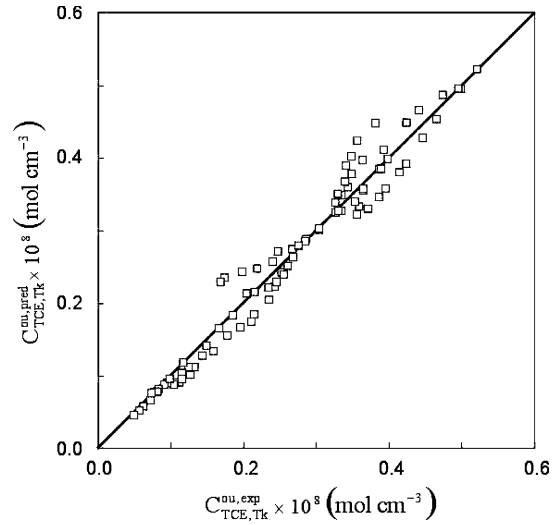

Figure 10. Results considering deposition and catalyst agglomeration with model iii and all runs. Predicted values $C^{ou,pred}_{TCE,Tk}(t)$ versus experimental values $C^{ou,exp}_{TCE,Tk}(t)$. Experimental data (□): $C_{m,cat.} = 1.0$ g/L, $C^0_{TCE} = 52.32$ mg L^{-1}; $C_{m,cat.} = 0.50$ g/L, $C^0_{TCE} = 35.75$ mg L^{-1}; $C_{m,cat.} = 0.50$ g/L, $C^0_{TCE} = 65.08$ mg L^{-1}; $C_{m,cat.} = 1.0$ g/L, $C^0_{TCE} = 24.02$ mg L^{-1}; $C_{m,cat.} = 0.25$ g/L, $C^0_{TCE} = 42.8$ mg L^{-1}; $C_{m,cat.} = 0.50$ g/L, $C^0_{TCE} = 15.46$ mg L^{-1}; $C_{m,cat.} = 0.25$ g/L, $C^0_{TCE} = 65.08$ mg L^{-1}; $C_{m,cat.} = 1.0$ g/L, $C^0_{TCE} = 68.43$ mg L^{-1}; $C_{m,cat.} = 0.25$ g/L, $C^0_{TCE} = 21.7$ mg L^{-1}.

the TCE degradation. It has been useful to show that reactor wall deposition produced by the characteristics of titanium dioxide and catalyst agglomeration resulting from the fluid circulation and variations in the suspension pH by the reaction products seriously interferes with predictions from theoretical model simulations.

(3) It has been shown that, under realistic operating conditions, the mechanical and optical properties of the employed catalyst operated in a slurry reactor become a function of time.

(4) The employed system was an annular, tubular reactor inside a recycle; three different models, assuming an increasing degree of complexity were employed: (i) the perfectly mixed system, (ii) the tubular reactor operating at pseudo-steady-state, and (iii) the tubular reactor operating at transient state. Only the third one, after consideration of deposition and agglomeration effects, improved the correspondence of the theoretical predictions with the experimental results.

Acknowledgment

Thanks are given to Universidad Nacional del Litoral, CONICET, and FONCYT (ANPCYT) for financial help. The technical assistance of Engineer Claudia Romani is gratefully appreciated.

Nomenclature

a_V = solid−liquid interfacial area per unit reactor volume (cm^2 mL^{-1})
C = molar concentration (mol mL^{-1})
C_m = mass concentration (g mL^{-1})
D = diameter (cm)
$D_{i,mix}$ = diffusion coefficient of i-species in the mixture (cm^2 s^{-1})
$D_e = 2(r_{ou} - r_{in})$, equivalent diameter (cm)
e^a = local volumetric rate of photon absorption (einstein mL^{-1} s^{-1})
$\underline{e}$ = unit vector along the coordinates axes (dimensionless)
i = current intensity (A)
I = specific radiation intensity (einstein s^{-1} cm^{-2} sr^{-1})
L = length (cm)

p = phase function (dimensionless)
Q = volumetric flow rate (mL s^{-1})
r = cylindrical radial coordinate (cm)
$\boldsymbol{R}_{het}$ = heterogeneous reaction rate (mol cm^{-2} s^{-1})
S_g = catalyst surface area (cm^2 g^{-1})
t = time (s)
t_R = mean residence time (s)
v = velocity (cm s^{-1})
V = volume (mL)
$\underline{x}$ = position vector (cm)
z = cylindrical axial coordinate (cm)

Greek Letters

α = kinetic parameter (mol cm^{-2} $g^{1/2}$ $einstein^{-1/2}$ $s^{-1/2}$)
α_3 = kinetic parameter (mL mol^{-1})
$\beta = \sigma + \kappa$, volumetric extinction coefficient (cm^{-1})
ϕ = cylindrical coordinate (rad)
Φ = quantum yield (mol $einstein^{-1}$)
ε_L = liquid hold-up (dimensionless)
$\eta = \underline{e}_z \cdot \underline{\Omega} = \cos \gamma_z$ (dimensionless)
$\kappa = \kappa^* C_m$, volumetric absorption coefficient (cm^{-1})
κ^* = mass absorption coefficient (cm^2 g^{-1})
λ = wavelength (cm)
$\mu = \underline{e}_r \cdot \underline{\Omega} = \cos \gamma_r$ (dimensionless)
$\sigma = \sigma^* C_m$, volumetric scattering coefficient (cm^{-1})
σ^* = mass scattering coefficient (cm^2 g^{-1})
$Y = I/I_0$, transmission coefficient (dimensionless)
$\underline{\Omega}$ = unit vector in the direction of propagation (dimensionless)
Ω = solid angle (sr)
ν = stoichiometric coefficient (dimensionless)
$\tau = t/t_R$, dimensionless time (dimensionless)

Subscripts

0 = initial condition
bs = relative to backscattering
cat. = relative to the catalyst
ext = relative to the outer wall of the external annular space
i = relative to the i-species
in = relative to the inner wall
Lp = relative to lamp
ou = relative to the outer wall
r = relative to the r-axis
Rf = relative to reflection
R = relative to the reactor
Tk = relative to the storage tank
tot. = total value
z = relative to the z-axis
λ = dependence on wavelength
Ω = relative to the direction of radiation propagation

Superscripts

0 = initial condition
in = inlet value
init = initial value
e = relative to emission
exp = experimental value
pred = value predicted by the model
ou = outlet value
t = denotes time parametric dependence
* = denotes specific property (per unit mass)

Special Symbols

$\langle\rangle$ = average value
$\cdot$ = dot product

Literature Cited

(1) Hoffmann, M. R.; Martin, S. T.; Choi, W.; Bahnemann, D. W. Environmental Applications of Semiconductor Photocatalysis. *Chem. Rev.* **1995**, *95*, 69.

(2) Herrmann, J. M. Heterogeneous Photocatalysis: Fundamentals and Applications to the Removal of Various Types of Aqueous Pollutants. *Catal. Today* **1999**, *53*, 115.

(3) Bahnemann, D. W. Photocatalytic Water Treatment: Solar Energy Applications. *Sol. Energy* **2004**, *77*, 445.

(4) Satuf, M. L.; Brandi, R. J.; Cassano, A. E.; Alfano, O. M. Scaling-up of Slurry Reactors for the Photocatalytic Degradation of 4-Chlorophenol. *Catal. Today* **2007**, *129*, 110.

(5) Sgalari, G.; Camera-Roda, G.; Santarelli, F. Discrete Ordinate Method in the Analysis of Radiative Transfer in Photocatalytically Reacting Media. *Int. Commun. Heat Mass Transfer* **1998**, *25*, 651.

(6) Duderstad, J.; Martin, W. *Transport Theory*; Wiley: New York, 1979.

(7) Salaices, M.; Serrano, B.; De Lasa, H. I. Photocatalytic Conversion of Organic Pollutants. Extincion Coefficients and Quantum Efficiencies. *Ind. Eng. Chem. Res.* **2001**, *40*, 5455.

(8) Salaices, M.; Serrano, B.; De Lasa, H. I. Experimental Evaluation of Photon Absorption in an Aqueous TiO_2 Slurry Reactor. *Chem. Eng. J.* **2002**, *90*, 219.

(9) Pareek, V. K.; Brungs, M. P.; Adesina, A. A. Photocausticization of Spent Bayer Liquor: A Pilot-Scale Study. *Adv. Environ. Res.* **2003**, *7*, 411.

(10) Pareek, V. K.; Cox, S. J.; Brungs, M. P.; Young, B.; Adesina, A. A. Computational Fluid Dynamic (CFD) Simulation of a Pilot-Scale Annular Bubble Column Photocatalytic Reactor. *Chem. Eng. Sci.* **2003**, *58*, 859.

(11) Jeon, J. H.; Kim, S. D.; Lim, T. H.; Lee, D. H. Degradation of Trichloroethylene by Photocatalysis in an Internally Circulating Slurry Bubble Column Reactor. *Chemosphere* **2005**, *60*, 1162.

(12) Toepfer, B.; Gora, A.; Li Puma, G. Photocatalytic Oxidation of Multicomponent Solutions of Herbicides: Reaction Kinetics Analysis with Explicit Photon Absorption Effects. *Appl. Catal., B* **2006**, *68*, 171.

(13) Li Puma, G.; Brucato, A. Dimensionless Analysis of Slurry Photocatalytic Reactors Using Two-Flux and Six-Flux Radiation Absorption-Scattering Models. *Catal. Today* **2007**, *122*, 78.

(14) Li Puma, G.; Yue, P. L. A Novel Fountain Photocatalytic Reactor for Water Treatment and Purification: Modeling and Design. *Ind. Eng. Chem. Res.* **2001**, *40*, 5162.

(15) Qazaq, S.; Hudaya, T.; Lee, I. A. L.; Sudilis, A.; Adesina, A. A. Photoremediation of Natural Leachate from a Municipal Solid Waste Site in a Pilot-Scale Bubble Column Reactor. *Catal. Commun.* **2007**, *8*, 1917.

(16) Romero, R. L.; Alfano, O. M.; Cassano, A. E. Radiation Field in an Annular, Slurry Photocatalytic Reactor. 2. Model and Experiments. *Ind. Eng. Chem. Res.* **2003**, *42*, 2479.

(17) Brandi, R. J.; Citroni, M. A.; Alfano, O. M.; Cassano, A. E. Absolute Quantum Yields in Photocatalytic Slurry Reactors. *Chem. Eng. Sci.* **2003**, *58*, 979.

(18) Brandi, R. J.; Rintoul, G.; Alfano, O. M.; Cassano, A. E. Photocatalytic Reactors—Reaction Kinetics in a Flat Plate Solar Simulator. *Catal. Today* **2002**, *76*, 161.

(19) Cabrera, M. I.; Negro, A. C.; Alfano, O. M.; Cassano, A. E. Photocatalytic Reactions Involving Hydroxyl Radical Attack: II. Kinetics of the Decomposition of Trichloroethylene Using Titanium Dioxide. *J. Catal.* **1997**, *172*, 380.

(20) Satuf, M. L.; Brandi, R. J.; Cassano, A. E.; Alfano, O. M. Experimental Method To Evaluate the Optical Properties of Aqueous Titanium Dioxide Suspensions. *Ind. Eng. Chem. Res.* **2005**, *44*, 6643.

(21) Brandi, R. J.; Alfano, O. M.; Cassano, A. E. Rigorous Model and Experimental Verification of the Radiation Field in a Flat-Plate Solar Collector Simulator Employed for Photocatalytic Reactions. *Chem. Eng. Sci.* **1999**, *54*, 2817.

(22) Brandi, R. J.; Alfano, O. M.; Cassano, A. E. Evaluation of Radiation Absorption in Slurry Photocatalytic Reactors. 2. Experimental Verification of the Proposed Method. *Environ. Sci. Technol.* **2000**, *34*, 2631.

(23) Prudent, A. L.; Ollis, D. F. Photoassisted Heterogeneous Catalysis: The Degradation of Trichloroethylene in Water. *J. Catal.* **1983**, *82*, 404.

(24) Brandi, R. J. Modelado de Fotorreactores con Partículas en Suspensión para Tratamiento de Contaminantes Orgánicos. Ph.D. Dissertation, Universidad Nacional del Litoral, Santa Fe, Argentina, 1998.

(25) Satuf, M. L.; Brandi, R. J.; Cassano, A. E.; Alfano, O. M. Quantum Efficiencies of 4-Chlorophenol Photocatalytic Degradation and Mineralization in a Well-Mixed Slurry Reactor. *Ind. Eng. Chem. Res.* **2007**, *46*, 43.

(26) Cabrera, M. I.; Alfano, O. M.; Cassano, A. E. Absorption and Scattering Coefficients of Titanium Dioxide Participate Suspensions in Water. *J. Phys. Chem.* **1996**, *100*, 20043.

(27) Ballari, M. d. l. M.; Brandi, R. J.; Alfano, O. M.; Cassano, A. E. Mass Transfer Limitations in Photocatalytic Reactors Employing Titanium Dioxide Suspensions: II. External and Internal Particle Constrains for the Reaction. *Chem. Eng. J.* **2008**, *136*, 242.

(28) Cassano, A. E.; Alfano, O. M. Reaction Engineering of Suspended Solid Heterogeneous Photocatalytic Reactors. *Catal. Today* **2000**, *58*, 167.

(29) Cassano, A. E.; Martín, C. A.; Brandi, R. J.; Alfano, O. M. Photoreactor Analysis and Design: Fundamentals and Applications. *Ind. Eng. Chem. Res.* **1995**, *34*, 2155.

(30) Wolfrum, E. J.; Turchi, C. S. Comments on: Reactor Dynamics in the Evaluation of Photocatalytic Oxidation Kinetics. *J. Catal.* **1992**, *136*, 626.

(31) Ballari, M. d.l. M.; Brandi, R. J.; Alfano, O. M.; Cassano, A. E. Mass Transfer Limitations in photocatalytic Reactors Employing Titanium Dioxide Suspensions: I. Concentration Profiles in the Bulk. *Chem. Eng. J.* **2008**, *136*, 50.

(32) Romero, R. L.; Alfano, O. M.; Cassano, A. E. Cylindrical Photocatalytic Reactors. Radiation Absorption and Scattering Effects Produced by Suspended Fine Particles in an Annular Space. *Ind. Eng. Chem. Res.* **1997**, *36*, 3094.

(33) Satuf, M. L. Modelado y Verificación Experimental de la Cinética de Degradación de un Contaminante Orgánico en Medio Acuoso Empleando Reactores Fotocatalíticos de Lecho Suspendido. Ph.D. Dissertation, Universidad Nacional del Litoral, Santa Fe, Argentina, 2006.

Received for review March 3, 2009
Revised manuscript received July 13, 2009
Accepted September 7, 2009

IE900354Y